[7] Godsave, G. A. E., "Studies of the combustion of drops in a fuel spray—the burning of single drops of fuel," *Fourth Symposium (International) on Combustion* (Williams and Wilkins Co., Baltimore, Md., 1953), p. 818.

[8] Wise, H., Lorrell, J., and Wood, B. J., "The effects of chemical and physical parameters on the burning rate of a liquid droplet," *Fifth Symposium (International) on Combustion* (Reinhold Publishing Co., New York, 1955), p. 132.

[9] Wood, B. J., Wise, H., and Inami, S. H., "Heterogeneous combustion of multicomponent fuels," Combust. Flame **4**, 235–242 (1960).

[10] Agoston, G. A., Wise, H., and Rosser, W. A., "Dynamic factors affecting the combustion of liquid spheres," *Sixth Symposium (International) on Combustion* (Reinhold Publishing Co., New York, 1957), p. 708.

[11] Berlad, A. L. and Hibbard, R. R., "Effect of radiant energy on vaporization and combustion of liquid fuels," NACA RM E52I09 (November 13, 1952).

[12] Isoda, H. and Kumagai, S., "New aspects of droplet combustion," *Seventh Symposium (International) on Combustion* (Butterworths Scientific Publications, London, 1959), p. 523.

[13] Milne-Thompson, L. M., *Theoretical Hydrodynamics* (Macmillan Co., New York, 1960), p. 452.

[14] Savic, P., "Hydrodynamical and heat transfer problems of liquid spray droplets," Quart. Bull., Gas Dynamics Div., Natl. Res. Council (January 1–March 31, 1953).

[15] Wise, H. and Ablow, C. M., "Burning of a liquid droplet, III: Conductive heat transfer within the condensed phase during combustion," J. Chem. Phys. **27**, 389–393 (1957).

[16] Lorell, J., Wise, H., and Carr, R. E., "Steady-state burning of a liquid droplet, II: Bipropellant flame," J. Chem. Phys. **25**, 325–331 (1956).

MAY 1963 AIAA JOURNAL VOL. 1, NO. 5

Free-Molecule Flow and Convective-Radiative Energy Transport in a Tapered Tube or Conical Nozzle

E. M. Sparrow* and V. K. Jonsson†
University of Minnesota, Minneapolis, Minn.

An analysis is presented of the fluid flow and heat transfer characteristics of a highly rarefied gas passing through a tapered tube or conical nozzle. The rate of mass throughflow has been determined as a function of the pressures and temperatures of the system and of the tube dimensions. It is found that, at moderate and large angles of taper, the mass throughflow is affected little by increases in tube length, except for short tubes. At small taper angles, the mass throughflow is more sensitive to tube length. The energy transport analysis includes simultaneous convection and radiation. Numerical results have been found for the adiabatic wall temperature. It is found that, for surfaces that can be approximated realistically as diffuse emitters and reflectors of thermal radiation, the results differ little from those for pure radiation.

Nomenclature

A = surface area
A_1 = tube cross section, small end
A_2 = tube cross section, large end
a = accommodation coefficient
e = convective energy/time-area
F = angle factor
f = solution of Eq. (3)
g = solution of Eq. (5)
L = tube length
M = rate of mass throughflow
m = mass flux/time-area
p = pressure
q = local heat flux/time-area
R = gas constant
r_1 = tube radius, small end
r_2 = tube radius, large end
T = absolute temperature
x = axial coordinate
α = absorptivity
β = ratio of convective to radiative efflux
γ = specific heat ratio
ϵ = emissivity
θ = half-taper angle
Λ = vertex to entrance distance
ξ = axial distance from vertex
σ = Stefan-Boltzmann constant
τ = temperature variable

Subscripts

1 = chamber 1
2 = chamber 2
r,rad = radiative
c = convective

Introduction

THE internal flow of rarefied gases has been a subject of study for over half a century. Almost all of the work has been concerned with parallel-walled conduits such as the circular tube and the flat rectangular duct. Only very recently has attention been directed to less elementary passage shapes, for instance, Refs. 1 and 2. Of particular interest among these is the tapered tube or conical nozzle, which includes the circular tube as a special case.

The paper is concerned with both the fluid flow and the heat transfer characteristics of a highly rarefied gas passing through a tapered tube or conical nozzle. The density level is such that collisions among molecules of the gas are much less probable than are collisions between the gas molecules

Received by IAS November 21, 1962; revision received April 1, 1963. The authors gratefully acknowledge the cooperation of the Numerical Analysis Center of the University of Minnesota. Their research was supported in part by the National Science Foundation, Grant G-10117.

* Professor of Mechanical Engineering, Heat Transfer Laboratory, Department of Mechanical Engineering.

† Research Assistant, Heat Transfer Laboratory, Department of Mechanical Engineering.

and the bounding walls (i.e., the molecular mean free path is much larger than a typical dimension of the apparatus). This is called the regime of free-molecule flow. At these low densities the convective energy transport is reduced greatly, and this circumstance requires that any complete heat transfer analysis include the effects of thermal radiation between the bounding walls. Such an analysis including simultaneous convection and radiation is presented herein.

The free-molecule fluid flow problem for the tapered tube or conical nozzle has been studied previously in Ref. 1. The analysis was confined to short tubes, and the problem was formulated within the framework of the Monte Carlo-random walk method. In the present study, a fundamentally different formulation of the problem is carried out. Use is made of an analogy between the molecular transport of mass and energy in a low-density gas and the transport of energy by thermal radiation. This analogy was discussed in a general way in Ref. 3 and was extended and illustrated in Ref. 4 by application to the circular tube, which is a special case of the tapered-tube system considered here. A comparison of the present results with those of Ref. 1 indicates agreement only for very short tubes. For the longer of the tubes considered in Ref. 1, the agreement is not too good, and this well may be because of the approximate nature of the Monte Carlo calculation. The present investigation is concerned generally with tubes much longer than those of Ref. 1.

The problem of energy transport in a tapered tube, within the knowledge of the authors, has not been studied previously. There are a variety of specific problems that might be considered, depending upon the thermal boundary conditions that are imposed at the tube surface. Here, attention will be directed to the problem of the adiabatic wall and, specifically, to finding the temperature distribution along the wall as a function of system pressures, temperatures, and dimensions.

A schematic diagram of the tapered-tube system is presented in Fig. 1. The tube is of length L and has radii r_1 and r_2, respectively, at its small and large ends. The angle of taper is 2θ. The coordinate x measures the axial distance along the tube from its small end. The tube connects two large chambers that are of sufficient size so that equilibrium conditions exist within each. The reflection of mass at the tube surface and the emission and reflection of thermal radiation all are assumed to be diffuse. The fluid-flow analysis will be presented first, with the energy transport analysis to follow later.

Fluid-Flow Analysis

Mathematical Formulation

The goal of the forthcoming analysis is to determine the net mass flow passing through the tapered tube or conical nozzle as a function of system pressures, temperatures, and dimensions. The first step in the analysis is to find the distribution of the mass flux incident and reflected at the tube wall as a function of position along the tube. It is useful to note that, under free-molecule flow conditions, the molecular stream that originates in the left-hand chamber is unaffected by the molecular stream that originates in the right-hand chamber. Consequently, each molecular stream can be treated independently. One begins by treating first the stream that originates in the left-hand chamber. The results for the simultaneous action of both streams can be found later by direct linear superposition.

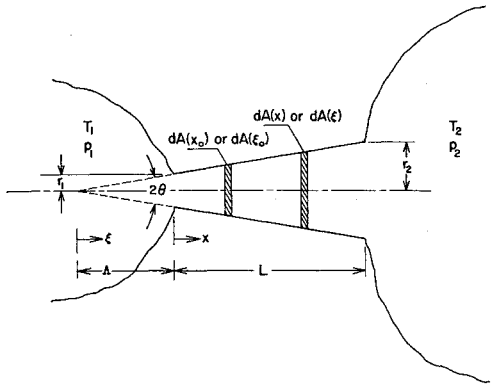

Fig. 1 Schematic of the tapered tube (conical nozzle) system

At a typical location x_0 [area $dA(x_0)$] on the tube wall, the conservation principle requires that the rate at which mass is incident on the wall element must be equal to the rate at which mass streams away from the element. The incident mass comes from two distinct zones: directly from the chamber 1, and by reflection from all other surface elements on the tube wall. Under the assumption of equilibrium within the chamber 1 (i.e., Maxwellian distribution function), the mass streaming into the tube per unit time and area at $x = 0$ is

$$m_1 = p_1/(2\pi R T_1)^{1/2} \tag{1}$$

This mass is distributed uniformly and diffusely across the tube entrance. Making use of the analogy with thermal radiation (for instance, see Ref. 4), the amount of this incoming mass which is directly incident per unit time and unit area at x_0 is

$$m_1 F_{dA(x_0)-1} \tag{2a}$$

in which $F_{dA(x_0)-1}$ is an angle factor.‡

In addition, if $m(x)$ represents the rate at which reflected mass leaves a surface element per unit area at location x, then the analogy with thermal radiation indicates that an amount§ $m(x)\ dF_{dA(x_0)-dA(x)}$ arrives per unit time and unit area at x_0. But mass arrives at x_0 by reflection from all locations along the tube, and the overall rate is given by the integral

$$\int_{x=0}^{L} m(x)\ dF_{dA(x_0)-dA(x)} \tag{2b}$$

The mass flux incident at $dA(x_0)$ per unit time and area is obtained by summing expressions (2a) and (2b), and this must equal the leaving mass flux $m(x_0)$; thus

$$f(x_0) = F_{dA(x_0)-1} + \int_0^L f(x) dF_{dA(x_0)-dA(x)} \tag{3}$$

in which

$$f = m/m_1 \tag{4}$$

Equation (3) represents a linear integral equation that must be solved to obtain f or m.

If an analysis similar to the foregoing is carried out for the molecular stream that originates in the right-hand chamber 2, there is derived

$$g(x_0) = F_{dA(x_0)-2} + \int_0^L g(x) dF_{dA(x_0)-dA(x)} \tag{5}$$

$$g = m/m_2$$

The incoming mass flux m_2 is found by exchanging subscripts 1 for 2 in Eq. (1). It might appear that separate solutions would have to be found for Eqs. (3) and (5). However, as will be demonstrated now, such is not the case. By the conservation principle, mass leaving $dA(x_0)$ will either pass out

‡ $F_{dA(x_0)-1}$ represents that fraction of the diffuse radiation leaving area $dA(x_0)$ which arrives at the disk (area = πr_1^2) stretched across the opening of chamber 1.

§ $dF_{dA(x_0)-dA(x)}$ represents that fraction of the diffuse radiation leaving area $dA(x_0)$ which arrives at another element $dA(x)$ on the wall.

through the openings at $x = 0$ and $x = L$ or else will strike at other locations on the tube wall; thus

$$F_{dA(x_0)-1} + F_{dA(x_0)-2} + \int_0^L dF_{dA(x_0)-dA(x)} = 1 \quad (6)$$

After substituting into Eq. (5) and rearranging, there follows

$$1 - g(x_0) = F_{dA(x_0)-1} + \int_0^L [1 - g(x)]dF_{dA(x_0)-dA(x)} \quad (7)$$

From a comparison with Eq. (3), it is seen that

$$g(x) = 1 - f(x) \quad (8)$$

Therefore, to find the wall mass flux distribution g corresponding to influx from chamber 2, it is sufficient to solve Eq. (3) for the f distribution corresponding to influx from chamber 1.

For the situation in which mass streams simultaneously into the tube from both chambers, direct superposition gives $m = m_1 f + m_2 g$. Introducing m_1 and m_2 from Eq. (1) and using (8), there is obtained

$$m(x) = [p_1/(2\pi RT_1)^{1/2}]f(x) + [p_2/(2\pi RT_2)^{1/2}][1 - f(x)] \quad (9)$$

With this, the net throughflow of mass through the tube can be calculated. Let M denote the net rate of mass flow from chamber 1 to chamber 2. Clearly, M is equal to the mass streaming out of chamber 1 into the tube minus the mass that streams back into the chamber. The latter quantity includes both mass reflected at the tube wall and mass that passes directly from chamber 2 to chamber 1 without contact at the tube walls:

$$M = m_1A_1 - m_2A_2F_{2-1} - \int_{x=0}^L m(x)dF_{dA(x)-1} \quad (10)$$

in which $A_1 = \pi r_1^2$ and $A_2 = \pi r_2^2$. This expression may be rephrased by noting that by the reciprocity rule

$$A_2F_{2-1} = A_1F_{1-2}$$

$$A_1 \int_0^L dF_{1-dA(x)} = \int_0^L F_{dA(x)-1}\, dA(x) \quad (11a)$$

and also that by the conservation principle

$$F_{1-2} = 1 - \int_0^L dF_{1-dA(x)} \quad (11b)$$

Employing these and substituting for $m(x)$ from Eq. (9), there follows

$$\frac{M/\pi r_1^2}{[1/(2\pi R)^{1/2}][p_1/(T_1)^{1/2} - p_2/(T_2)^{1/2}]} =$$

$$1 - \frac{1}{\pi r_1^2} \int_{x=0}^L f(x)F_{dA(x)-1}dA(x) \quad (12)$$

It is seen from Eq. (12) that the evaluation of the mass throughflow requires a knowledge of the function f that solves Eq. (3). These solutions will be examined now.

Angle Factors

Before solutions of Eq. (3) can be found, it is necessary to know the angle factors $F_{dA(x_0)-1}$ and $dF_{dA(x_0)-dA(x)}$. These quantities are unavailable in the literature and will be derived below. For this derivation, it is convenient to introduce an auxiliary coordinate ξ that measures axial distance from the (virtual) vertex of the tapered tube. From Fig. 1, it easily is seen that

$$x = \xi - \Lambda \qquad x_0 = \xi_0 - \Lambda \qquad \Lambda = r_1/\tan\theta \quad (13)$$

Consideration is given first to the angle factor $F_{dA(x_0)-1}$ between a ring element of tube surface at x_0 [area $dA(x_0)$; see Fig. 1] and a circular disk stretched across the tube at $x = 0$.

The starting point of the derivation is the well-known angle factor for diffuse interchange between two parallel, coaxial circular disks [for instance, Ref. 5, Eq. (31-45)]. If the disks are separated by a distance h and have radii r_a and r_b, the disk-to-disk angle factor F_{d-d} for radiation passing from r_a to r_b is

$$F_{d-d} = \{h^2 + r_a^2 + r_b^2 - [(h^2 + r_a^2 + r_b^2)^2 - 4r_a^2r_b^2]^{1/2}\}/2r_a^2 \quad (14)$$

This may be applied to disks spanning the cross section at $x = 0$ and $x = x_0$: these have radii $\Lambda\tan\theta$ and $\xi_0\tan\theta$, respectively. By setting $r_a = \Lambda \tan\theta$ and $r_b = \xi_0 \tan\theta$, there follows after some manipulation

$$F_{d-d}(1,x_0) = \{\Lambda^2 + \xi_0^2 - 2\Lambda\xi_0 \cos^2\theta - (\xi_0 - \Lambda) \times [(\xi_0 + \Lambda)^2 - 4\xi_0\Lambda \cos^2\theta]^{1/2}\}/2\Lambda^2 \sin^2\theta \quad (15)$$

This is the fraction of the mass entering the tube at $x = 0$ which passes through the cross section at x_0. Similarly, the fraction of the entering mass which passes through the cross section at $(x_0 + dx_0)$ is $F_{d-d}\ (1,\ x_0 + dx_0)$. The difference between $F_{d-d}\ (1,x_0)$ and $F_{d-d}(1,x_0 + dx_0)$ must be equal to the fraction of the entering mass which is directly incident on the ring $dA(x_0)$; thus

$$F_{1-dA(x_0)} = F_{d-d}(1,x_0) - F_{d-d}(1,x_0 + dx_0) = -(\partial F_{d-d}/\partial\xi_0)d\xi_0 \quad (16)$$

Then, by applying the reciprocity rule,

$$F_{dA(x_0)-1} = [A_1/dA(x_0)]F_{1-dA(x_0)} = -[A_1/dA(x_0)] \times (\partial F_{d-d}/\partial\xi_0)d\xi_0 \quad (17a)$$

This may be evaluated by differentiating Eq. (15) with respect to ξ_0 and replacing $[A_1/dA(x_0)]d\xi_0$ by $\Lambda^2 \sin\theta/2\xi_0$. The end result of these operations is

$$F_{dA(x_0)-1} = \left\{\frac{(\xi_0 - \Lambda)^2 + \Lambda(3\xi_0 - \Lambda)\sin^2\theta}{[(\xi_0 - \Lambda)^2 + 4\xi_0\Lambda \sin^2\theta]^{1/2}} - (\xi_0 - \Lambda) - \Lambda \sin^2\theta\right\} \Big/ 2\xi_0 \sin\theta \quad (17b)$$

This is the desired angle factor between a ring element at x_0 and the opening of the tube into chamber 1.

The angle factor $dF_{dA(x_0)-dA(x)}$ between two ring elements on the tube wall may be derived in an analogous manner. The disk-to-disk angle factor, Eq. (14), is applied first to a pair of disks spanning the tube cross section at x and x_0; this provides an expression for $F_{d-d}(x,x_0)$. By pursuing arguments similar to the foregoing, one finds that

$$dF_{dA(x_0)-dA(x)} = -\frac{\sin\theta}{2\xi_0}\frac{\partial}{\partial\xi}\left(\xi^2\frac{\partial F_{d-d}}{\partial\xi_0}\right)d\xi \quad (18a)$$

and after differentiating

$$dF_{dA(x_0)-dA(x)} = \frac{\cos^2\theta}{2\xi_0 \sin\theta}\left\{1 - |\xi_0 - \xi| \times \frac{(\xi_0 - \xi)^2 + 6\xi_0\xi \sin^2\theta}{[(\xi_0 - \xi)^2 + 4\xi_0\xi \sin^2\theta]^{3/2}}\right\} d\xi \quad (18b)$$

As a final step, the angle factor expressions may be placed in dimensionless form. When this has been done, it is found that two parameters appear: the half-angle of taper θ and and the tube aspect ratio L/r_1. It will be necessary to specify numerical values of these for each solution of Eq. (3).

Distribution of Mass Incident on the Wall

Consideration now may be given to the solution of Eq. (3). Closed-form solutions could not be found, and numerical means were employed instead. The numerical

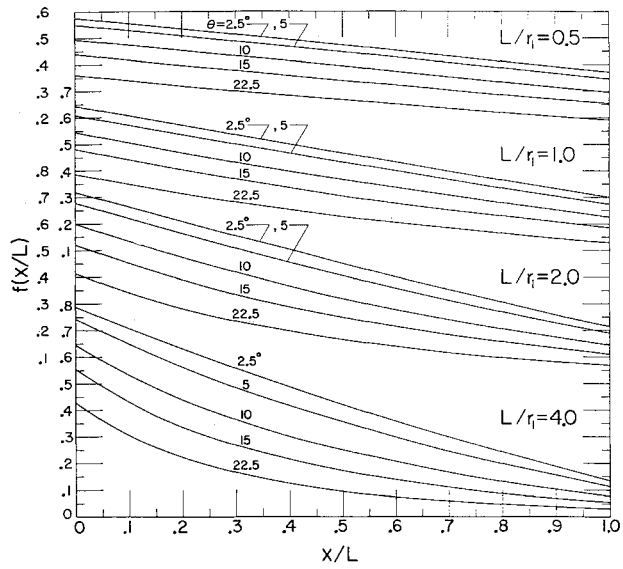

Fig. 2a The f function for the mass flow problem, smaller L/r_1

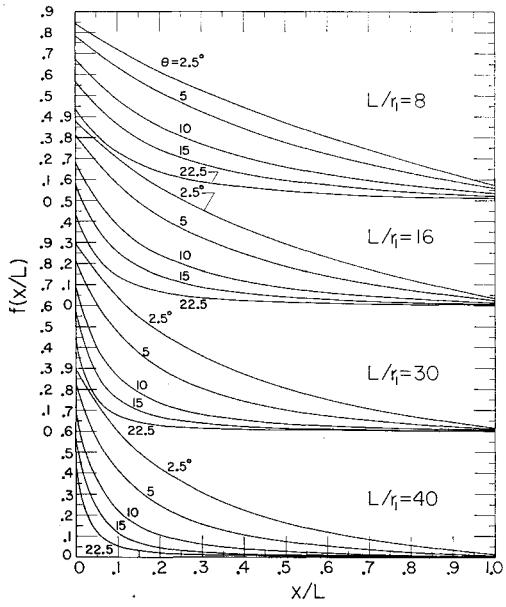

Fig. 2b The f function for the mass flow problem, larger L/r_1

technique was one of successive iteration, and this was carried out on a Control Data 1604 electronic computer. The general procedure was similar to that already described in Ref. 4 for the circular tube. At no time during the calculations was there any difficulty in achieving convergence.

Solutions of Eq. (3) were carried out for values of the half-taper angle θ of 0°, 2.5°, 5°, 10°, 15°, and 22.5°. For each one of these, L/r_1 was assigned values of 0.5, 1, 2, 4, 8, 16, 30, and 40. The distributions of f which thus are obtained are plotted in Figs. 2a and 2b as a function of position along the tube. The first of the figures is for the shorter tubes, whereas the latter is for the longer tubes. Each one of the figures contains a number of grids, each of which corresponds to a particular L/r_1 and has its own ordinate scale. The abscissa scale is common to all of the grids.

In interpreting the results of Fig. 2, it should be recalled that f represents the distribution of mass flux incident on the tube wall corresponding to an incoming mass flux m_1 at $x = 0$. As expected, the greatest incidence of mass flux occurs near the tube entrance at $x = 0$. The mass flux decreases continuously with increasing axial distance, but at a rate that depends strongly on geometrical parameters. In particular, for short tubes and small angles of taper, the mass flux distribution does not vary too much along the length of the tube. However, as the taper angle increases, there is a substantial variation of f even for short tubes; for instance, for $L/r_1 = 1$ and $\theta = 22.5°$, f varies from 0.39 to 0.13, a drop-off of two thirds. For tubes of moderately short lengths, the f variation is large at all angles; for instance, for $L/r_1 = 4$ and $\theta = 5°$, f varies from 0.74 to 0.12. For longer tubes, the variation of f along the length becomes even greater, with especially sharp drop-offs occurring for the tubes with greater taper.

The large variations of f along the length of the tube serve to justify the effort of solving the integral equation. It would be expected that any approximate method based on the assumption that f is distributed uniformly over the tube length would lead to large errors.

Mass Throughflow Results

The net mass throughflow M now can be evaluated from Eq. (12). These results have been plotted as solid lines in Fig. 3 as a function of the tube aspect ratio L/r_1 for parametric values of half-taper angle θ. Also appearing in the figure are dashed lines that represent the results computed in Ref. 1 by the Monte Carlo method. Additionally, there is a dot-dash line that represents the asymptote for long circular tubes, for which the right side of Eq. (12) has the value $\frac{8}{3}/(L/r_1)$.

Inspection of Fig. 3 reveals several interesting trends. First of all, under fixed pressure and temperature conditions, the mass flow decreases with increasing tube length for a tube of given taper. However, the rate of this decrease depends very strongly on the angle of taper. For tubes with large taper angle, an increase in tube length has very little influence on the mass flow, except in the case of very short tubes. For smaller angles of taper, the mass flow becomes more sensitive to increases in tube length. In the limit for $\theta = 0$ (circular tube), the mass flow decreases inversely with L for long tubes. Generally speaking, the mass flow in tubes of given length and inlet radius r_1 is larger when the angle of taper θ is larger.

It is seen additionally that the direction of the net flow is from the chamber having the higher value of $p/T^{1/2}$ to the chamber having the lower value of $p/T.^{1/2}$ This is true regardless of the taper angle, i.e., regardless of whether $r_1 > r_2$ or $r_2 > r_1$. For the isothermal condition $T_1 = T_2$, the flow direction is from high to low pressure. On the other hand, when $p_1 = p_2$, the flow direction is from low to high temperature.

A comparison of the present results (solid lines) with the Monte Carlo calculation (dashed lines) indicates agreement only for very short tubes. For the longest tubes calculated by the Monte Carlo method, $L/r_1 \sim 10$, the agreement is not good, with errors as large as 20% for the smallest angles of taper. Insufficient calculation details are given in Ref. 1 to permit an appraisal of the reasons for this disparity. It

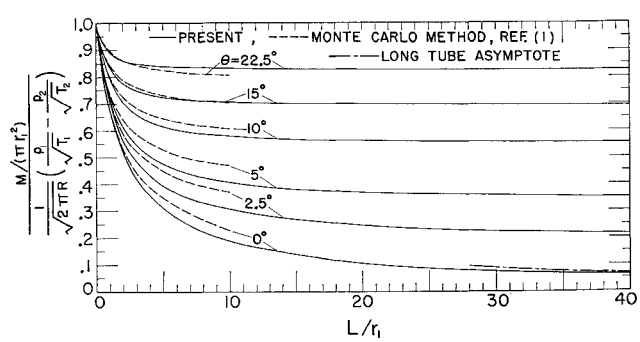

Fig. 3 Results for the mass throughflow

well may be related to the approximate nature of the Monte Carlo method. The present calculations have been checked very carefully, and it is the expectation of the authors that the present results as presented in Fig. 3 are accurate to well within 1%.

Energy Transfer Analysis

A general formulation of the heat transfer problem for arbitrary thermal boundary conditions will be carried out first. Later, consideration will be given to the case of the adiabatic wall.

General Formulation

The net heat transfer q per unit time and area at an elemental area on the tube wall may be written as the sum of the contributions due to thermal radiation q_r and free-molecule convection q_c:

$$q = q_r + q_c \tag{19}$$

in which all quantities are positive when heat flows out of the surface element. It next is necessary to relate the q_r and q_c to the thermal and flow parameters of the system. These derivations are quite lengthy, and only a general outline will be given here.

Considering first the net radiative heat flux q_r at a typical location x_0, there are the following contributions to be accounted for: 1) the emission from the element $\epsilon\sigma T^4(x_0)$; 2) the radiation from the chambers 1 and 2 which is directly incident and is absorbed at x_0; and 3) the radiation emitted and reflected at all other locations on the tube wall which arrives and is absorbed at x_0. Under the condition of thermal equilibrium within the chambers, the radiation streaming into the tube at either end is blackbody radiation. The rate at which energy from chamber 1 arrives per unit area at x_0 is $\sigma T_1^4 F_{dA(x_0)-1}$. Of this, a fraction α is absorbed. Similarly, from chamber 2, thermal radiation arrives at x_0 at a rate $\sigma T_2^4 F_{dA(x_0)-2}$ per unit area, and a fraction α is absorbed. The absorbed energy flux described in item 3 requires a rather lengthy derivation, the end result of which is

$$\epsilon \int_0^L \sigma T^4 dF_{dA(x_0)-dA(x)} - (1-\alpha) \times \int_0^L q_r(x) dF_{dA(x_0)-dA(x)} \tag{20}$$

In the derivation of expression (20), it has been assumed that both emitted and reflected radiation is diffusely distributed, i.e., Lambert's cosine law is obeyed. Upon collecting the various energy quantities discussed in the foregoing and assuming graybody conditions ($\alpha = \epsilon$), there results

$$q_r(x_0) = \alpha\sigma T^4(x_0) - \alpha\sigma[T_1^4 F_{dA(x_0)-1} + T_2^4 F_{dA(x_0)-2}] - \int_0^L [\alpha\sigma T^4(x) - (1-\alpha) q_r(x)] dF_{dA(x_0)-dA(x)} \tag{21}$$

The net heat flux q_c due to free-molecule convection is derived most easily by analogy with the radiation balance of Eq. (21). To accomplish this, it is necessary to introduce several new quantities. One of these is the thermal accommodation coefficient a, which measures the extent to which mass incident on a surface is brought into thermal equilibrium with it. Valuable discussions of the numerical values of the accommodation coefficient and their experimental determination may be found in Refs. 6 and 7. It has been shown[4] that the role of a in the convective-transport problem is analogous to the role of α in the radiative-transport problem. Furthermore, the blackbody thermal radiation from the chambers is analogous to the convective fluxes e_1 and e_2, as given below:

$$e_{1,2} = 0.5R[(\gamma+1)/(\gamma-1)] m_{1,2} T_{1,2} \tag{22}$$

in which m_1 and m_2 are defined by Eq. (1). Finally, the local emissive power $\sigma T^4(x_0)$ at x_0 is analogous to the fully accommodated convective flux $e(x_0)$:

$$e(x_0) = 0.5R[(\gamma+1)/(\gamma-1)] m(x_0) T(x_0) \tag{23}$$

The local mass flux $m(x_0)$ has been derived in the initial part of this paper and is given by Eq. (9). By making use of the analogous quantities just described in conjunction with Eq. (21), there follows

$$q_c(x_0) = ae(x_0) - a[e_1 F_{dA(x_0)-1} + e_2 F_{dA(x_0)-2}] - \int_0^L [ae(x) - (1-a) q_c(x)] dF_{dA(x_0)-dA(x)} \tag{24}$$

If the surface temperature were prescribed, then Eqs. (21) and (24) would serve as integral equations from which q_r and q_c could be determined, respectively. It may be noted that Eqs. (21) and (24) are completely independent of one another for prescribed wall temperature. For the case in which the heat flux q is prescribed, the situation is more complex, since, in general, q_r and q_c would not be known a priori.

Adiabatic Wall

At this point, attention will be directed to the case of the adiabatic wall, for which $q = 0$ and $q_r = -q_c$ at every surface element. After considerable manipulation, q_r and q_c can be eliminated from Eqs. (21) and (24) with the aid of the condition $q = 0$. From this, there results a single integral equation for the distribution of the adiabatic wall temperature:

$$\alpha\sigma T^4(x_0) + ae(x_0) - \Omega(x_0) = \sigma \int_0^L T^4(x) [\alpha(2-a) dF_{dA(x_0)-dA(x)} - \alpha(1-a) dK(x_0,x)] + \int_0^L e(x) [a(2-\alpha) dF_{dA(x_0)-dA(x)} - a(1-\alpha) dK(x_0,x)] \tag{25}$$

in which $\Omega(x_0)$ represents a known function of x_0:

$$\Omega(x_0) = [\alpha\sigma T_2^4 + ae_2] dF_{dA(x_0)-2} - [\alpha(1-a)\sigma T_2^4 + a(1-\alpha)e_2] \times \int_0^L F_{dA(x)-2} dF_{dA(x_0)-dA(x)} + [\alpha\sigma T_1^4 + ae_1] dF_{dA(x_0)-1} - [\alpha(1-a)\sigma T_1^4 + a(1-\alpha)e_1] \int_0^L F_{dA(x)-1} dF_{dA(x_0)-dA(x)}$$

and dK is an abbreviation for

$$dK(x_0,x) = \int_{x'=0}^{L} dF_{dA(x')-dA(x)} dF_{dA(x_0)-dA(x')}$$

with x' a dummy integration variable. Considering the foregoing, it is quite apparent that the governing equation for the adiabatic wall temperature distribution is highly complex. First of all, the equation is highly nonlinear, with the temperature appearing as T and T^4. Additionally, if dimensionless variables are used, it is found that there are seven independent parameters that would have to be specified for each solution:

$$\begin{array}{cccc} T/_2T_1 & p_2/p_1 & L/r_1 & \theta \\ \beta_1 = e_1/\sigma T_1^4 & \alpha & a & \end{array} \tag{26}$$

Of these, only β_1 may be somewhat unfamiliar, and this will be discussed later. The large number of parameters is an especially serious drawback if numerical solutions are being contemplated. A minimum exploration of two values of each parameter would lead to 128 cases. Clearly, the computational effort for such a highly complex mathematical system would be enormous.

For the special case in which $\alpha = a$, a significant simplification occurs. Upon adding together Eqs. (21) and (24), it is found that heat flux terms appear only as the sum $q_r + q_c$, whereas temperature terms appear only as a sum $e +$

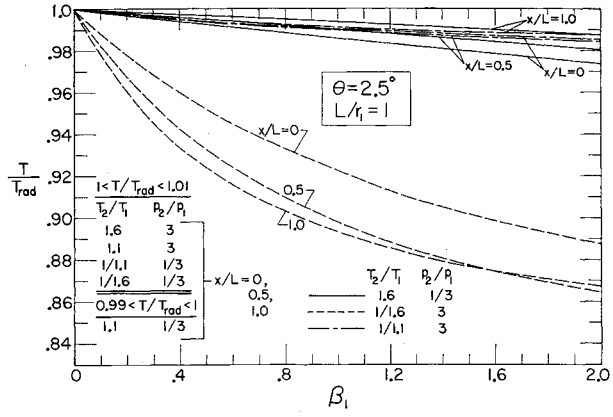

Fig. 4a Illustrative adiabatic wall temperatures, $L/r_1 = 1$, $\theta = 2.5°$

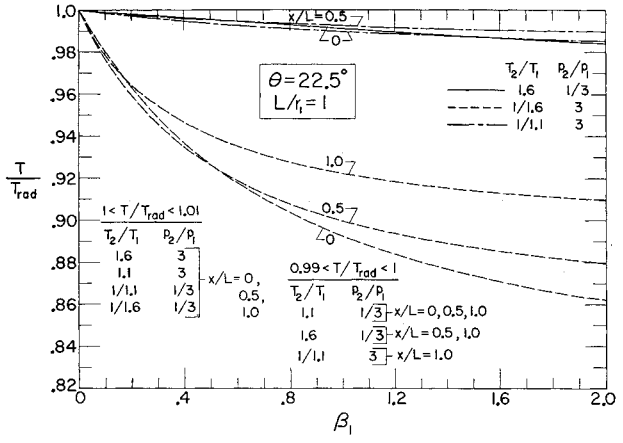

Fig. 4b Illustrative adiabatic wall temperatures, $L/r_1 = 1$, $\theta = 22.5°$

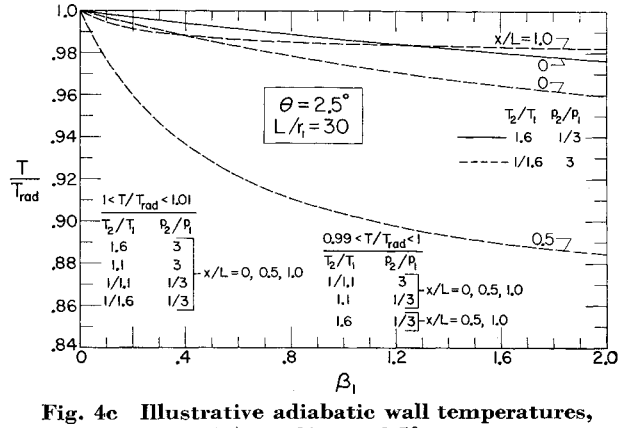

Fig. 4c Illustrative adiabatic wall temperatures, $L/r_1 = 30$, $\theta = 2.5°$

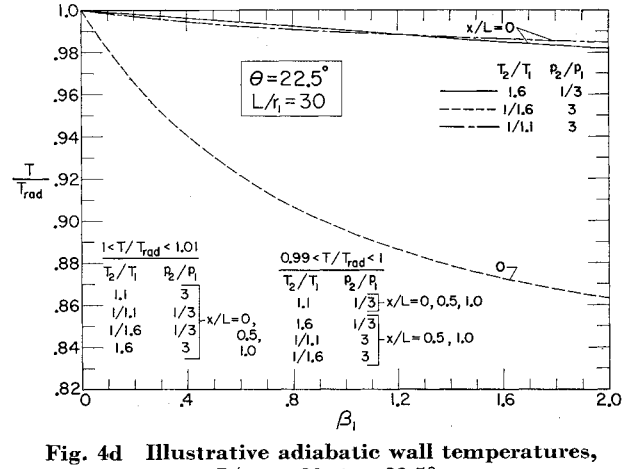

Fig. 4d Illustrative adiabatic wall temperatures, $L/r_1 = 30$, $\theta = 22.5°$

σT^4. If the former sum is equated to zero and the latter is replaced by a new temperature variable

$$\tau = e + \sigma T^4 \tag{27}$$

there follows

$$\tau(x_0) = \tau_1 F_{dA(x_0)-1} + \tau_2 F_{dA(x_0)-2} + \int_0^L \tau(x) dF_{dA(x_0)-dA(x)} \tag{28}$$

The foregoing is a linear integral equation for the temperature variable τ, the solutions for which can be shown to depend on two parameters, θ and L/r_1. Comparing Eq. (28) with Eq. (25), the relative simplicity of the former is clearly evident. Inasmuch as numerical solutions are involved, the drastic reduction in the number of parameters is especially important. In addition, the linearity of Eq. (28) makes it more amenable to numerical solution.

In deciding on a reasonable direction for the numerical work, it is appropriate to look at the properties of typical engineering materials. Surfaces that may be expected to emit and reflect infrared radiation in an approximately diffuse manner include nonmetals, metallic oxides, and perhaps very rough metallic surfaces. Such surfaces have moderate or high values for the absorptivity coefficient α. Highly polished metallic surfaces tend to be specular-type reflectors (i.e., mirrors) and are characterized by low values of α, usually below 0.1. Therefore, an analytical model based on diffusely distributed radiation should be confined realistically to moderate or high α values. Furthermore, experimental values of the accommodation coefficient a for various gases on engineering surfaces that have not been cleaned physically and chemically and purged of adsorbed gases tend to be high. In the light of the foregoing discussion, it would appear that the values of α and a appropriate to an analysis based on diffusely distributed radiation should not be greatly different.

In a first attack on any problem, it is natural to consider the simplest cases from which insights can be obtained about the physical phenomena. Taking the foregoing discussion into consideration and recalling the complexity of the mathematical system represented by Eq. (25), the authors are persuaded that Eq. (28) is a more appropriate starting point for numerical consideration than is Eq. (25). From the results to be presented in later paragraphs it will be seen that, for surfaces that realistically can be considered diffuse, there is little motivation to pursue the refinements (i.e., $\alpha \neq a$) contained in Eq. (25).

Now, turning to Eq. (28), it is seen that, because of its linearity, it can be split up into two equations, one with inhomogeneous term $\tau_1 F_{dA(x_0)-1}$ and the other with inhomogeneous term $\tau_2 F_{dA(x_0)-2}$. The first of these is essentially the same as Eq. (3) for the f function, whereas the second is essentially the same as Eq. (5) for the g function. Using the solution of these prior equations, the solution for τ can be written as

$$\tau = \tau_1 f(x) + \tau_2 [1 - f(x)] \tag{29}$$

Then, introducing the definitions of τ and e from Eqs. (27, 22, and 23) and evaluating $m(x)$,m_1, and m_2 from Eqs. (9) and (1), there follows after some rearrangement

$$\left[\frac{T(x)}{T_1}\right]^4 + \beta_1 \left\{ f(x) + \frac{p_2}{p_1}\left(\frac{T_1}{T_2}\right)^{1/2} [1 - f(x)] \right\} \frac{T(x)}{T_1} =$$

$$(1 + \beta_1) f(x) + [1 - f(x)] \left[\beta_1 \frac{p_2}{p_1} \left(\frac{T_2}{T_1}\right)^{1/2} + \left(\frac{T_2}{T_1}\right)^4 \right] \tag{30}$$

The foregoing is a fourth-degree algebraic equation for determining the adiabatic wall temperature as a function of position along the tube wall. Solutions of this quartic can be obtained conveniently by finding the roots of the resolvent cubic as described in Ref. 8. There are five parameters to

be prescribed: $T_2/T_1, p_2/p_1, \beta_1, L/r_1$, and θ. Thus, in any reasonable amount of space, it is impossible to display the complete parametric dependence of the adiabatic wall temperature. Within the limitations of space, the best that can be done is to consider some illustrative cases in order to establish some feel for the trends. Before proceeding with this, it is worth while discussing the range of the β_1 parameter.

As indicated in Eq. (26), β_1 represents the ratio of the convective and radiative effluxes from chamber 1, i.e., $e_1/\sigma T_1^4$. If e_1 is evaluated from Eqs. (22) and (1), the expression for β_1 becomes

$$\beta_1 = \frac{1}{2(2\pi)^{1/2}} \frac{(\gamma + 1)}{(\gamma - 1)} \frac{p_1(RT_1)^{1/2}}{\sigma T_1^4} \tag{31}$$

For air at a temperature of 500°R (room temperature), $\beta_1 = 10^5 p$ (atm). For tube dimensions on the order of 0.1 in., p should be no greater than 5×10^{-6} atm (about 4 μ Hg) in order to achieve free-molecule conditions, whereas, for dimensions no the order of 1 in., p should not exceed 5×10^{-7} atm (about 0.4 μ Hg). The values of β_1 corresponding to these two cases are 0.5 and 0.05 for $T = 500$°R. It further may be noted that $\beta_1 \sim T_1^{-3.5}$. So, β_1 will decrease quite rapidly when the temperature level is raised above room temperature. On the other hand, at temperature levels below room temperature, β_1 will be larger.

Now, consideration can be given to illustrating the parametric dependence of the adiabatic wall temperature. To this end, Figs. 4a–4d have been prepared. The first two of these figures are meant to typify a short tube, $L/r_1 = 1$, with Fig. 4a corresponding to a small taper angle and Fig. 4b corresponding to a large taper angle. The last two of the figures are meant to typify a long tube, $L/r_1 = 30$, with Figs. 4c and 4d, respectively, corresponding to small and large taper angles. On the ordinate of each figure, there is plotted the ratio of the adiabatic wall temperature at some x location to the adiabatic wall temperature for pure radiation‖ at that same x. The temperature ratio T_2/T_1 is assigned values of 1.1, 1.6, 1/1.1, 1/1.6, and the pressure ratio p_2/p_1 is given values of 3 and $\frac{1}{3}$. The range of β_1 on the abscissa is from 0 to 2, although it is recognized that only the left-hand part of the figures is appropriate to temperature levels that do not go below room temperature. Results for $x/L = 0$, 0.5, and 1 are given on Figs. 4.

For most of the cases investigated, T/T_{rad} differed from unity by less than 1%. To preserve the clarity of the figures, curves were not plotted for these cases; rather, they are tabulated. An overall inspection of the figures indicates that interesting deviations of T/T_{rad} from unity appear to occur only when $p_2 \gg p_1$ and when $T_2 \ll T_1$—in other words, when the gas entering the large end of the tube is at an appreciably higher pressure and an appreciably lower temperature than the gas entering the small end of the tube. Since $\beta_1 \sim p_1$, it is highly unlikely that large values of p_2/p_1 and large values of β_1 will occur simultaneously. In addition, when T_2 is appreciably less than T_1, it is quite unlikely that T_1 will be below room temperature. Therefore, for the situation in which $p_2 \gg p_1$ and $T_2 \ll T_1$, it would appear that the β_1 values will be much lower than those estimated in an earlier paragraph. For instance, if $p_2/p_1 = 3$ and if the pressure p_2 is such to provide free-molecule flow conditions when the large end of the tube has a dimension of 0.1 in., then $\beta_1 = (\frac{1}{3})(0.5) \cong 0.17$ for room temperature conditions. If, on the other hand, the pressure p_2 is such to provide free-molecule conditions when the large end of the tube has a dimension of 1 in., then $\beta_1 = (\frac{1}{3})\ (0.05) \cong 0.017$. Using these β_1 values, it easily is verified from Figs. 4 that the one situation that appeared, at first glance, to offer interesting deviations of T/T_{rad} from unity does, in fact, lead to T/T_{rad} only slightly different from unity. Closer inspection of the figures reveals that, for very short tubes, T/T_{rad} does not depend strongly on position, whereas the opposite is true for long tubes. This is physically reasonable.

In light of the foregoing, the authors are led to the conclusion that the adiabatic wall temperature can be calculated without appreciable error by considering only the radiative transport. This conclusion applies to surfaces that can be approximated realistically as diffuse emitters and reflectors of thermal radiation. For highly polished metallic surfaces, which are specular reflectors, it cannot be said with any certainty that the forementioned conclusion still applies. An analytical approach altogether different from that given here would have to be employed in the specular case.

‖ T_{rad} is calculated from Eq. (30) after deleting terms containing β_1.

References

[1] Davis, D. H., Levenson, L. L., and Milleron, M., "Theoretical and experimental studies of molecular flow through short ducts," *Advances in Applied Mechanics, Supplement 1, Rarefied Gas Dynamics* (Academic Press Inc., New York, 1961), pp. 99–115.

[2] Kruger, C. H. and Shapiro, A. H., "The axial-flow compressor in the free-molecule range," *Advances in Applied Mechanics, Supplement 1, Rarefied Gas Dynamics* (Academic Press Inc., New York, 1961), pp. 117–140.

[3] Eckert, E. R. G., "Similarities between energy transport in rarefied gases and by thermal radiation," *Modern Developments in Heat Transfer*, edited by W. E. Ibele (Academic Press Inc., New York, 1963), pp. 159–180.

[4] Sparrow, E. M., Jonsson, V. K., and Lundgren, T. S., "Free-molecule tube flow and adiabatic wall temperature," Am. Soc. Mech. Engrs. Paper 62-HT-35 (1962); also J. Heat Transfer (to be published).

[5] Jakob, M., *Heat Transfer* (John Wiley and Sons Inc., New York, 1957), Vol. 2, p. 14.

[6] Hartnett, J. P., "A survey of thermal accommodation coefficients," *Advances in Applied Mechanics, Supplement 1, Rarefied Gas Dynamics* (Academic Press Inc., New York, 1961), pp. 1–28.

[7] Wachman, H. Y., "The thermal accommodation coefficient: a critical survey," ARS J. **32**, 2–12 (1962).

[8] Burington, R. S., *Handbook of Mathematical Tables and Formulas* (Handbook Publishers, Sandusky, Ohio, 1940), pp. 8–9.